Hard magnets based on transition metal complexes with the dicyanamide anion, $\{N(CN)_2\}^-$†,‡

Mohamedally Kurmoo*,§,[a] and Cameron J. Kepert§,[b]

[a] *Institut de Physique et Chimie des Matériaux de Strasbourg (GMI) (CNRS UMR 7504), 23 Rue du Loess, F-67037 Strasbourg cedex, France*
[b] *Inorganic Chemistry Laboratory, University of Oxford, South Parks Road, Oxford, UK OX1 3QR*

We present the crystal structures and magnetic properties of a series of magnetic compounds, $M^{II}\{N(CN)_2\}_2$, where M = Cu (**1**), Ni (**2**), Co (**3**) and Fe (**4**), and $[Mn\{N(CN)_2\}_2(C_2H_5OH)_2]Z\cdot(CH_3)_2CO$ (**5**). In the isostructural compounds **1**–**4**, the dicyanamide anion is triply coordinating through its three nitrogen atoms. It bridges the metal ions to form infinite 3D metal-organic frameworks with a rutile-type structure. The framework contains doubly bridged $M(-N\equiv C-N-C\equiv N-)_2$ ribbons that link approximately orthogonally through the amide nitrogen atoms. The Jahn–Teller distortion in **1** has a strong influence on the packing arrangement (M—N bond lengths: 1.98 and 2.47 Å for **1** and 2.10 and 2.15 Å for **3**). On lowering the temperature the bond distances in **1** remain unchanged except for a decrease of the $M-N_{amide}$ length to 2.45 Å. Magnetic data for **1** obey the Curie–Weiss law ($\Theta = -2.1$ K). **2** and **3** are ferromagnets with Curie temperatures (T_C) of 9 and 21 K and are characterized by hysteresis loops of 710 and 7975 Oe at 2 K, remnant magnetization, magnetization approaching the expected saturation (gS) of 2 and 3 μ_B in high field, absorptive component (χ'') in the AC magnetization and λ peak in the heat capacity data. **4** is similarly characterized and shows behaviour that is characteristic of a canted antiferromagnet: the Weiss constant is temperature dependent (+3 K in the range 200–300 K), there is a sharper peak than for **1** or **2** in the AC magnetization and the isothermal magnetization at 3 K increases monotonically to ≈ 1.3 μ_B (expected to be 4 μ_B for ferromagnetic alignment of the spins) in a field of 8 T. Its coercive field (17 800 Oe) is the largest observed for any metal-organic compound and exceeds those of alloys of $SmCo_5$ and $Nd_2Fe_{14}B$. The maximum energy product ($B \cdot H$) is the highest for **3** and is comparable to alloys of Sm–Co. We attribute the large coercive field to a combination of single ion and particle shape anisotropies. **5** is paramagnetic at high temperature with $\Theta = -3$ K. Below 16 K it behaves as a canted antiferromagnet with a very weak resultant spontaneous magnetization.

Considerable interest has recently arisen in the engineering of infinite metal-organic polymeric frameworks, a principle aim being the construction of architectures with novel chemical, physical and mechanical properties.[1] In the area of organic electronics there is a strong drive towards materials with combined properties for opto-electronic, magneto-optical and magneto-conducting devices. Our own interest over the past few years has been devoted to the search for a magnetic superconductor where the electronically active component is an organic moiety, such as a TTF (tetrathiafulvalene) derivative, and where the localized moments reside on an inorganic part, such as an anionic transition metal complex.[2] We have recently synthesized stable organic-inorganic hybrid salts (BEDT-TTF)$_4$AFe$(C_2O_4)_3\cdot C_6H_5CN$ [where A = K^+, NH_4^+ or H_2O; BEDT = bis(ethylenedithio)] that contain paramagnetic layers of $[AM^{III}(C_2O_4)_3]$ sandwiched between conducting BEDT-TTF layers.[3] The A = H_2O salt is a superconductor with a critical temperature of 8 K, while the K^+ and NH_4^+ salts are semiconductors. Recently, Kini and coworkers reported the highest T_c ever reached by a donor-based organic superconductor in salts of BEDT-TTF having diamagnetic, polymeric anion layers of the form $[Cu^I\{N(CN)_2\}X]^-$ (X = Cl^- or Br^-).[4] These exciting and promising discoveries prompted us to seek related species by replacing Cu^+ in $[Cu\{N(CN)_2\}X]^-$ (X = Cl^-, Br^- or CN^- [5]) with paramagnetic transition metals.

Complexation of dicyanamide to Ni^{II} was reported by Köhler *et al.*[6] to yield species of the form $[Ni\{N(CN)_2\}_4]^{2-}$, $[Ni\{N(CN)_2\}_3]^-$ and $[Ni_2\{N(CN)_2\}_5]^-$. The latter two were proposed to have polymeric structures. In repeating these syntheses we obtained a light blue complex, $Ni\{N(CN)_2\}_2$, also described by Köhler and colleagues,[7] which behaves as a ferromagnet below 21 K. Consequently, we prepared the Cu (**1**), Co (**3**) and Fe (**4**) analogs and performed systematic studies of their crystal structures and their optical and magnetic properties. The results for the series $M^{II}\{N(CN)_2\}_2$ are presented in this paper. Compounds **1**–**4** crystallize with a three-dimensional structure of the rutile-type. With the exception of **1**, all show spontaneous magnetization and have well-defined hysteresis loops below the Curie temperatures. In this paper, we also present the magnetic properties of a solvated adduct of the manganese salt (**5**), which is a canted antiferromagnet (weak ferromagnet) below 16 K. For this salt, we propose¶ a layer structure similar to that of $Co\{pyrimidine\}_2(NCS)_2$ and

† This work was presented in part at (*a*) the 58th Okazaki Conference on 'Recent Development and Future Prospect of Molecular Based Conductors', March 7–9, 1997, Institute of Molecular Science, Okazaki, Japan, (*b*) ISCOM 97, International Symposium on 'Crystalline Organic Metals, Superconductors and Ferromagnets', March 22–27, 1997, Sesimbra, Portugal and (*c*) NATO ARW on 'Supramolecular Engineering of Synthetic Metallic Materials: Conductors and Magnets', January 10–14, 1998, Sitges, Spain.

‡ Non-SI units employed: 1 bar = 10^5 Pa; I $\mu_B \approx 9.3 \times 10^{-24}$ J T^{-1}; 1 Oe $\approx$ 79.6 A m^{-1}.

§ E-mail: kurmoo@friss.u-strasbg.fr; cameron.kepert@chemistry.ox.ac.uk

¶ Following submission of this paper we have determined the structure of $[Mn\{N(CN)_2\}_2(C_2H_5OH)_2]\cdot(CH_3)_2CO$ and confirm the layered structure proposed

$Mn\{SCN\}_2(C_2H_5OH)_2$.[8,9]

The bis(dicyanamide)cobalt(II) and its pyridine adduct were also prepared by Köhler and coworkers.[7] They reported that a blue form of $Co\{N(CN)_2\}_2$ forms on heating the pink $Co\{N(CN)_2\}_2(py)_2$ under vacuum, whilst $Co\{N(CN)_2\}_2$ prepared from water forms as red crystals. The blue form was also obtained when the reaction was performed in dry acetone as solvent. Phenylarsonium salts of tris- and tetrakisdicyanamide cobaltate(II) have also been synthesized.[7b]

The synthesis of bis(dicyanamide)copper(II) has previously been reported.[6] Several adducts have subsequently been prepared and their optical, vibrational and magnetic properties studied.[10] In a few of these cases, weak ferromagnetic exchange was observed. In a very recent, communication, Batten *et al.* [11] reported the room temperature crystal structure of $Cu\{N(CN)_2\}_2$ and the observation of ferromagnetism in the cobalt and nickel complexes with T_C of 9 and 21 K, respectively. The coercive field of the nickel complex was found to be 191 Oe.

During an extensive study on the dicyanamide coordination complexes, we have observed exceptional magnetic properties, for example, a T_C of 56 K and coercive fields approaching 2 T. In the series of salts $M^{II}\{N(CN)_2\}_2$, where M is Cu, Ni, Co and Fe, we have established magnetic ordering with Curie temperatures reaching 21 K and coercive fields up to an unprecedented 18 000 Oe. We were able, for the first time, to tune these two parameters continuously, and as desired, by variation of the metal centres. Here we communicate the crystal structures of $M^{II}\{N(CN)_2\}_2$ (M = Cu and Co at 295 and 150 K), and the molecular structures (IR, Raman, EXAFS) and magnetic properties (AC, DC, hysteresis and heat capacity) of $M^{II}\{N(CN)_2\}_2$ (M = Cu, Ni, Co and Fe) and $[Mn\{N(CN)_2\}_2(C_2H_5OH)_2]\cdot(CH_3)_2CO$.

Experimental

Synthesis

All starting materials were reagent grade from Fluka and were used as received.

Two different methods were employed for the synthesis of the compounds with copper, nickel and cobalt. The first was the reaction at room temperature of aqueous solutions of transition metal nitrate hexahydrates with aqueous solutions of sodium dicyanamide, as described by Köhler and coworkers.[6,7] In general, gentle heating sped up the reaction rate. The microcrystalline complexes obtained by this method gave very well-defined powder X-ray diffraction patterns. Recrystallization of the powders (150 mg) from water (200 ml) over 3 and 9 months for copper and cobalt, respectively, gave fine needles with maximum dimensions of 0.4 and 0.5 mm. The second method, in which all reactions were carried out in absolute ethanol, was employed to produce fine micron-size powders. Solutions of the nitrate salt of the metals (3.0 g, 250 ml, $T < 10\,^{\circ}C$) and sodium dicyanamide (2.5 g, 250 ml, $T < 10\,^{\circ}C$) were mixed, and the temperature maintained below 10 °C. After 30 min, the solid sodium nitrate was filtered off and the filtrate warmed to 40 °C (except in the case of copper, where the filtrate was allowed to warm gently to room temperature) under vigorous mixing. The resulting fine turquoise green (Cu), pink (Co) and light blue (Ni) powders were filtered, washed with acetone and air-dried. Chemical analyses of the products for both synthetic routes were in very good agreement with the stoichiometry $M\{N(CN)_2\}_2$.

Compound **4** was prepared from iron sulfate heptahydrate by slight modification of the second method. All manipulations were carried out under an argon atmosphere. The starting materials were suspended in 500 ml of degassed ethanol and gently heated at 50 °C. White fibres of the product appeared after 2 h, and the reaction was continued until the iron sulfate had been consumed (approx. 2 h). The resulting creamy white powder contained $Fe\{N(CN)_2\}_2$ and Na_2SO_4. Since the product is very soluble in water and quite air-sensitive in solution, we did not manage to separate pure $Fe\{N(CN)_2\}_2$. Due to the slight solubility of $Fe\{N(CN)_2\}_2$ in ethanol the ratio $Fe\{N(CN)_2\}_2 : Na_2SO_4$ was *ca.* 1 : 1.6.

The manganese salt, $Mn\{N(CN)_2\}_2$, is highly soluble in water. Consequently, reaction of $[Mn(H_2O)_6](NO_3)_2$ with $Na\{N(CN)_2\}$ in water formed a viscous solution, which on drying produced impure $Mn\{N(CN)_2\}_2$ of poor quality. However, addition of an ethanol–acetone mixture to the viscous solution and storage at 5 °C for 24 h resulted in the formation of clear colourless crystals of $[Mn\{N(CN)_2\}_2(C_2H_5OH)_2]\cdot(CH_3)_2CO$. The crystals became opaque on filtration due to loss of solvent of crystallization.

Physical techniques

UV/VIS and vibrational spectroscopy. UV/VIS spectra (200–900 nm) were recorded by transmission at 295 K on a Hitachi U-3000 spectrometer. Samples were prepared by grinding the compounds in paraffin oil and dispersing the mixture between two pieces of optical quartz. Infrared spectra were recorded by transmission of a thin deposit of the compounds on a KBr plate by use of a Mattson FTIR spectrometer. The thin deposit was prepared by grinding the compounds in ethanol and allowing a drop to dry on the KBr plate. Far infrared and Raman spectra were recorded for us by Professor Y. Iwasa (JAIST, Kanazawa, Japan).

EXAFS (Extended X-ray absorption fine structure). K-edge transmission spectra of the metals were recorded at 80 K at the synchrotron ring at the Laboratoire pour l'Utilisation du Rayonnement Electromagnétique (LURE) in Orsay, France. The samples were prepared by dispersing *ca.* 10 mg of compound in 50 mg of cellulose.

TGA (Thermal gravimetric analysis). Data were collected in the temperature range 20 to 1100 °C by warming at 3 °C min^{-1} in air or argon on a Setaram TGA-92 calorimeter.

Heat capacity. Measurements were made on a home-built calorimeter that operates under pseudo adiabatic conditions. Samples (200–300 mg) were pelletized and mounted with grease on sapphire plates suspended by nylon wire. Due to the insulating nature of the samples a reasonable time was allowed for the heat pulse to dissipate until thermal equilibrium was attained at each temperature.

X-Ray data collection and analysis

Single crystal data collection and refinement. Single crystal X-ray refinement data were collected for $Cu\{N(CN)_2\}_2$ (**1**) at 150(2) and 295(2) K and for $Co\{N(CN)_2\}_2$ (**3**) at 150(2) K on an Enraf-Nonius DIP2000 diffractometer equipped with graphite-monochromated MoKα radiation, a nitrogen gas cryostream and Eu/Ba image plate detectors. Consecutive oscillations in ϕ (45 × 4° for **1**, 90 × 2° for **3**) were performed, and the images were processed with the HKL suite of programs.[12] Structures were solved by direct methods (SHELXS-86[13]) and refined by full matrix least-squares on F^2_{obs} (SHELXL-93[14]). All atoms were refined anisotropically. Important crystallographic data are summarised in Table 1.

The materials were found to be highly susceptible to twinning perpendicular to the *c*-direction, which is attributable to the near-equivalence of the *a* and *b* axes and the pseudo-mirror symmetry in planes of type {110}. We find that this source of twinning is less prevalent in **1**, where the angle between ribbons is increased due to the Jahn–Teller lengthening of the M—N(2) bond.

CCDC reference number 440/067.

Table 1 Summary of crystal data[a] for $M\{N(CN)_2\}_2$

	1	**1**	**2**	**3**[b]
Formula	$Cu\{N(CN)_2\}_2$	$Cu\{N(CN)_2\}_2$	$Ni\{N(CN)_2\}_2$	$Co\{N(CN)_2\}_2$
FW/g mol^{-1}	195.64	195.64	190.77	191.03
Measurement	Crystal	Crystal	Powder	Crystal
T/K	295(2)	150(2)	295(2)	150(2)
Space group	*Pnnm*	*Pnnm*	*Pnnm*	*Pnnm*
a/Å	6.120(1)	6.082(1)	5.980(1)	5.970(1)
b/Å	7.339(1)	7.288(1)	7.107(1)	7.060(1)
c/Å	7.173 (1)	7.187(1)	7.393(1)	7.406(1)
U/Å^3	322.17(8)	318.57(8)	314.2	312.15(8)
Z	2	2	2	2
ρ_{calcd}/M g^{-3}	2.017	2.040	2.017	2.032
$F(000)$	190	190		186
μ(MoKα)/mm^{-1}	3.317	3.355		2.674
Crystal size/mm	0.15 × 0.05 × 0.04	0.15 × 0.05 × 0.04		0.50 × 0.05 × 0.04
Mosaicity/°	0.5	0.5		0.4
$2\theta_{max}$/°	53.36	53.32		52.32
Total reflections	2966	2955		2124
Unique reflections	359	356		322
Reflections $I > 2\sigma(I)$	298	316		319
R(int)	0.053	0.047		0.018
Parameters	29	29		29
R indices [$I > 2\sigma(I)$]	$R_1 = 0.0293$	$R_1 = 0.0265$		$R_1 = 0.0182$
	$wR = 0.0643$	$wR = 0.0634$		$wR = 0.0590$
R indices (all data)	$R_1 = 0.0419$	$R_1 = 0.0352$		$R_1 = 0.0183$
	$wR = 0.0758$	$wR = 0.0797$		$wR = 0.0590$
Largest peaks/e Å^{-3}	0.53, −0.36	0.47, −0.39		0.28, −0.30

[a] From ref. 11: M = Cu, $a = 7.340$, $b = 6.1218$, $c = 7.1815$ Å; M = Ni, $a = 7.294$, $b = 6.024$, $c = 7.023$ Å; M = Co, $a = 7.301$, $b = 6.014$, $c = 7.073$ Å. [b] M = Co, $a = 5.964(1)$, $b = 7.029(1)$, $c = 7.294(1)$ Å (from neutron powder diffraction at 295 K on the D1B multidetector diffractometer of the Institut Laue Langevin, Grenoble).

Powder XRD (X-ray diffraction). Ground samples were pressed in a groove in a Perspex plate and mounted on a D500 or a D5000 Siemens X-ray powder diffractometer. Data were collected with monochromated Co- or Cu-Kα1 radiation, respectively. Data were collected in the range $2 < 2\theta < 100°$ using a step size of 0.02°. The unit cell parameters were obtained using TREOR and DICVOL91.[15]

Magnetic properties measurements

Faraday balance magnetometry. Measurements of the temperature dependent magnetic moments were made on a home-built pendulum system capable of operating with a maximum transverse field of 13 000 Oe. The system is equipped with a continuous flow cryostat operating down to 4 K. Polycrystalline samples (*ca.* 20 mg) were placed in gelatine capsules at the end of a quartz rod and data were collected in zero field and in an applied field of ≈1 T. Routine corrections were made for the contribution of the gelatine capsule and for the sample diamagnetism using Pascal's constants.

Vibrating sample magnetometry. The temperature dependence of the magnetization hysteresis loops and remnant magnetisation were recorded on a Princeton Applied Research vibrating sample magnetometer (model 155) having a maximum field of 18 000 Oe. The magnetometer is equipped with a He bath cryostat with an Oxford instruments ITC4 temperature controller. The powdered samples were held tightly in a Delrin container to prevent sample rotation.

SQUID (Superconducting quantum interference device) magnetometry. For measurements in near zero field (ZF) and for hysteresis loops at 2 K with fields greater than 1.5 T, two different SQUID magnetometers, Metronique and Quantum Design were used. The latter was also used to measure the AC susceptibilities.

Attempts to cool the samples in zero field using both SQUID magnetometers and using standard procedures (oscillation of the field for demagnetizing or quenching of the superconducting magnets), failed to give the expected zero magnetization at near zero temperature (2 K in our case). To eliminate all remnant field, we finally warmed the Metronique SQUID device to room temperature, allowed it to stand for over one month and then performed the magnetization measurements without ever applying a field. In each case we obtained a negative spontaneous magnetization. Our conclusion is that there is a small negative earth field trapped within the mu-metal shield of the cryostat. The magnetization data shown in Fig. 5 have been multiplied by −1 and normalised to the value at 2 K.

A comment is worth making here concerning sample support. For preliminary measurements made on samples held in gelatine capsules, systematic steps were observed in the hysteresis loops. We subsequently cemented the samples in polyethylene glycol (melting point ≈60 °C) to prevent motion of the particles. This procedure successfully removed all of the anomalies.

For the solvated manganese salt (**5**), an agglomerate of crystals with its solvent was placed in a gel cap, sealed and inserted in a clear drinking straw for measurement. The absolute value of the magnetization was calibrated to the amount of manganese in the sample determined by chemical analysis.

Results

From the chemical analyses there is consistently 0.5% hydrogen present in all of the compounds. This corresponds to 0.5 H_2O per formula unit, as proposed by Batten *et al.*[11] and Köhler and colleagues.[7] We found no evidence for water in our infrared data, and thermogravimetry shows only a small weight loss (<0.3%) below 100 °C, most likely coming from adsorbed moisture on the polycrystalline powders. The calculated solvent-accessible volume is zero for each structure,[16] indicating there are no regions lying between the van der Waals surface of the framework with enough volume to accommodate absorbed species.

Crystal structure

A summary of the crystal data and the bond lengths and angles are given in Tables 1 and 2. The dicyanamide is triply coordinating (Fig. 1), an arrangement that has not been observed in any of the other reported salts that contain this anion.[17] Apart from the free ion, such as in $Cs\{N(CN)_2\}$ and $(BEDT\text{-}TTF)_2\{N(CN)_2\}$,[18] the dicyanamide anion has previously shown three modes of coordination: singly coordinated[19] *via* one of its terminal nitrogen atoms as in $Ni(en)_2\{N(CN)_2\}_2$, $Cu(phen)\{N(CN)_2\}_2$ Cu(methyl imidazole)$_4\{N(CN)_2\}_2$; doubly coordinated by the two terminal nitrogen atoms as in $(CH_3)_2Sn(N(CN)_2)_2$, $(CH_3)_3Sn\{N(CN)_2\}$, $Ag\{N(CN)_2\}$, $Nd[\{N(CH_3)_2\}_3PO]_2[N(CN)_2]_3$[20] and $(BEDT\text{-}TTF)_2Cu\{N(CN)_2\}X$;[4,5] and quadruply coordinating in $(CH_3)_2Tl\{N(CN)_2\}$.[21] In the novel triple coordination observed here, the C(1)—N(2)—C(1) angle is considerably smaller than that observed previously (118.5° for **1** and 117.2° for **3**, compared to an average of 126° for the other structures).

The crystal structure of **1** is identical to that determined recently by Batten *et al.*[11] As such we will keep our discussions brief, only highlighting the main structural points and the effect of lowering the temperature. The structure of **3** has not been reported previously. A very close similarity of the powder X-ray diffraction patterns of **2** and **3** suggests closely similar structures for these complexes.

The crystal structures of $M^{II}\{N(CN)_2\}_2$ are based on close packing of linear ribbons that propagate along *c*. Within these ribbons, the dicyanamide forms double bridges between metal ions. Adjacent ribbons are slipped by half *c*, so that the apical amide nitrogen atoms complete the 4 + 2 coordination on the M^{II} ions (Fig. 2). The structure may alternately be viewed as a single network with connectivity identical to the rutile polymorph of TiO_2, where M and dicyanamide replace Ti and O. The asymmetry of the dicyanamide anion (and in **1**, the Jahn–Teller distortion of Cu^{II}) means that the structure is orthorhombic rather than tetragonal, and more closely related to $CrCl_2$.[22] In contrast, two *regular* rutile-type networks interpenetrate in $M^{II}\{C(CN)_3\}_2$ (where M = Zn, Cu, Ni, Co, Mn).[23]

The $M^{II}\{N(CN)_2\}_2$ structures distort from a regular tetragonal lattice to optimize van der Waals interaction distances between neighbouring dicyanamides (Table 2). This results in the bridged metal chains adopting a chair conformation, with the C1 and N2 lying out of the $MN1_4$ planes. The extent of this distortion determines the angle between neighbouring ribbons, and depends both on the choice of metal cation and on temperature. On cooling **1** from 295 to 150 K, the van der Waals interaction distances shorten due to a 40 to 45% decrease in thermal amplitudes (Table 2). There is also a considerable shortening of the Cu1–N2′ distance from 2.473(4) to 2.449(3) Å, whereas the equatorial Cu1—N1 bonds remain at 1.98 Å. These combined effects mean that the dihedral angle between the planes of neighbouring ribbons in **1** decreases from 52.3 to 50.2° for planes defined by N1, and from 69.2 to

Table 2 Bond lengths (Å) and angles (°) for $M\{N(CN)_2\}_2$

	$Cu\{N(CN)_2\}_2$	$Cu\{N(CN)_2\}_2$	$Co\{N(CN)_2\}_2$
T/K	295	150	150
Intramolecular			
M—N1	1.979(3)	1.980(2)	2.096(1)
M—N2	2.473(4)	2.449(3)	2.153(2)
N1—C1	1.144(4)	1.150(4)	1.152(2)
N2—C1	1.305(4)	1.309(3)	1.324(2)
N1—M—N1	87.5(2)	87.4(2)	85.13(9)
N1—M—N1	92.5(2)	92.6(2)	94.87(9)
N1—M—N2	88.6(1)	88.8(1)	88.95(6)
N1—M—N2	91.4(1)	91.2(1)	91.05(6)
C1—N1—M	158.4(3)	158.6(2)	159.91(14)
C1—N2—C1	118.5(2)	118.4(2)	117.2(2)
N1—C1—N2	174.0(3)	174.3(3)	175.3(2)
Intermolecular			
N1···N1	3.856(6)	3.787(5)	3.732(3)
N1···C1	3.811(4)	3.737(4)	3.750(2)
C1···C1	3.534(6)	3.451(5)	3.552(3)
C1···N2	3.617(5)	3.543(4)	3.769(3)
N2···N2	3.474(9)	3.404(8)	3.766(5)[a]

[a] Note the large increase of the N2···N2 distance due to slippage of the dicyanamide.

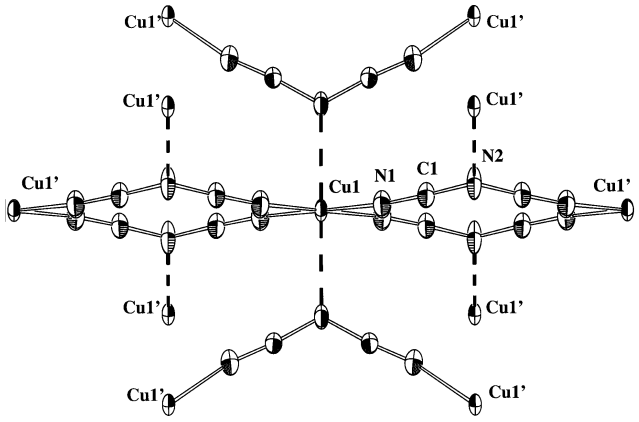

Fig. 1 Coordination of the triply coordinating dicyanamide anion to Jahn–Teller distorted Cu^{II} in **1** (axial bonds are represented by dashed lines). This unit forms the basis of an infinite 3D polymeric network that is closely related to the rutile structure. The four structurally independent atoms are labelled, as are all equivalent Cu atoms. Thermal ellipsoids are 50% probability for the 295 K structure

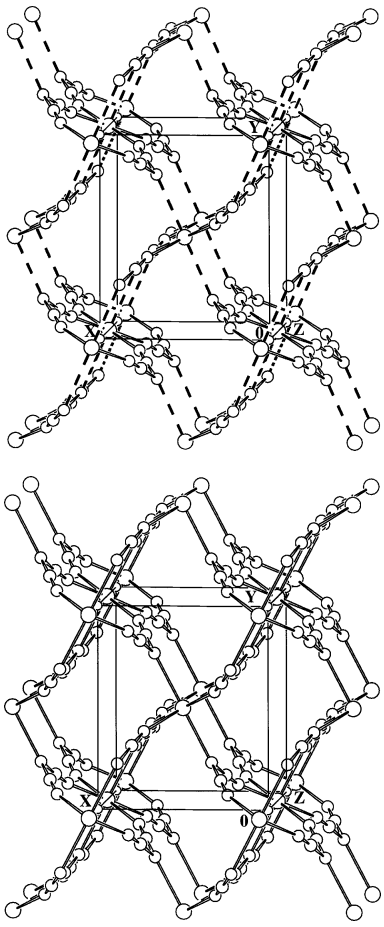

Fig. 2 Off-axis projection of the structure of (top) $Cu\{N(CN)_2\}_2$ and (bottom) $Co\{N(CN)_2\}_2$

68.1° for planes defined by N2. Correspondingly, the *a* and *b* axes shorten by 0.6 and 0.7%, respectively. Interestingly, there is an accompanying 0.2% lengthening in the *c* axis due to a decrease in librational motion within the ribbons.

Although complexes **2** and **3** are isostructural with **1**, their crystal structures differ significantly due to the absence of a strong Jahn–Teller distortion. In **3**, the M—M distance in the chain (Cu—Cu = 7.187 Å, *c* axis parameter) is increased to 7.406 Å due to an increase in the $M—N_{eq}$ distance from 1.98 (Cu) to 2.10 Å (Co). The reverse is seen for the *b* parameter, 7.288 (Cu) to 7.060 Å (Co), due to a decrease of the $M—N_{amide}$ distance from 2.45 (Cu) to 2.15 Å (Co). Most importantly, the distortion away from a regular tetragonal lattice is less severe in **2** and **3** than in **1**, and consequently the ribbons lie more closely orthogonal to one another (for **3**, the dihedral angle is 58.8° for planes defined by N1 and 79.1° for planes defined by N2). Furthermore, the intermolecular van der Waals interactions between dicyanamides differ significantly from those of **1** due to an effective slippage of these units (Table 2).

EXAFS

The EXAFS data were analysed by the Michalowicz suite of programs.[24] The oscillatory components of the fine structure of the spectra are shown in Fig. 3. The traces for **2**–**4** are superimposed to demonstrate the close similarity of the coordination sphere and the structure of the three complexes. This is in good agreement with the results of the powder X-ray diffraction.

UV/VIS and infrared spectra

The energies and assignments of the bands observed in the UV/VIS spectra of the compounds are given in Table 3. The absorption bands are, in general, very weak, as expected for ligand field transitions. The colours of the compounds and their corresponding spectra are consistent with octahedral coordination. The energies of the observed bands imply that the dicyanamide is a relatively weak-field ligand and lies between H_2O and NH_3 (or CH_3CN) in the spectrochemical series. This is consistent with the observed magnetic susceptibilities for high-spin metal ions.

Infrared and Raman spectra of the Co, Ni and Fe complexes are very similar, indicating closely related structures,[25] and are mutually exclusive, as expected for the metal ions in D_{2h} (2/*m*) site symmetry. The ligand vibrations (in cm^{-1}) at 2280, 2211 ν(C≡N), 1316 ν(N—C), 968 ν(N—C), 687 δ(N—C≡N), 527 γ(N—C≡N) and 504 δ(N—C≡N) have little dependence on the metal. In contrast, the low frequency bands vary quite strongly, the ν(M—N) band increasing with increasing mass of M. Two M—N stretching vibrations are observed in each spectrum, confirming the tetragonal distortion around the metals.

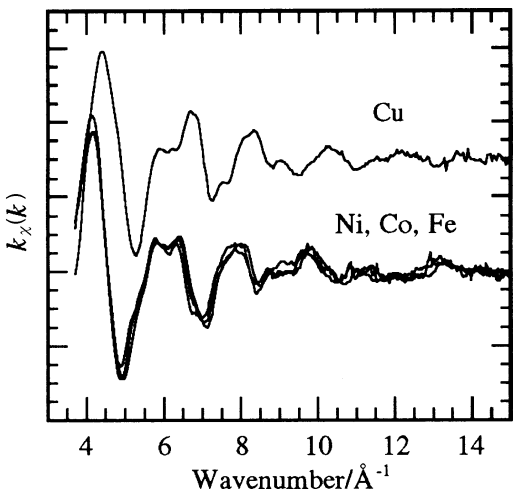

Fig. 3 Metal K-edge EXAFS oscillation functions $k\chi(k)$ of $M\{N(CN)_2\}_2$ measured at 80 K

Table 3 Assignments of the optical spectra[a] of $M\{N(CN)_2\}_2$

Metal	ν_{max}/cm^{-1}	Asssignment
Cu	14 600	$^2B_{1g} \rightarrow {}^2B_{2g}$
	27 000	$^2B_{1g} \rightarrow {}^2E_g$
Ni	16 300	$^3A_{2g} \rightarrow {}^3T_{1g}(F)$
	26 000	$^3A_{2g} \rightarrow {}^3T_{1g}(P)$
	34 000	
Co	19 400	$^4T_{1g}(F) \rightarrow {}^4A_{2g}(P)$
	21 000	$^4T_{1g}(F) \rightarrow {}^4T_{1g}(P)$
	31 250	
	34 500	
Fe	32 000	$^5T_{2g} \rightarrow {}^3T_{1g}$?
	39 500	$^5T_{2g} \rightarrow {}^3T_{2g}$?

[a] $[Mn\{N(CN)_2\}_2(C_2H_5OH)_2]\cdot(CH_3)_2CO$ does not show any spin-allowed absorption band in the visible range of the spectrum.

Magnetic properties

Paramagnetic region. The temperature dependence of the magnetic moment of compounds **1**–**5** are represented as the product of the susceptibility and temperature in Fig. 4. Appropriate details of the experimental conditions are given in the captions. The magnetic properties of the copper salt depend on the choice of synthetic route: $Cu\{N(CN)_2\}_2$ by the alcohol route shows a ferromagnetic interaction [$\Theta = +0.7(1)$ K], whilst the more highly crystalline material obtained by recrystallization from water (**1**) shows an antiferromagnetic interaction [$\Theta = -2.1(4)$ K] as reported by Batten *et al.*[11] Due to the lack of structural information on the former we will confine our discussion to the latter. The magnetic data of **1** were fitted to the Curie–Weiss law for the whole temperature range studied. No difference in behaviour between samples prepared by the two routes was observed for **2** and **3**. Above 100 K, the data for these salts can be fitted to the Curie–Weiss law with the parameters given in Table 4. The positive values of the Weiss constant for **2** and **3** suggest that ferromagnetic interactions dominate in these materials. The χT data for **4** show a very broad maximum; fitting of the high temperature data gives $\Theta = +3(1)$ K. This behaviour is difficult to interpret due to the large spin–orbit effect for high-spin Fe^{II}.[26] The data for the Mn complex (**5**) fit the Curie–Weiss law between 17 and 300 K with $\Theta = -3.0(1)$ K. The Curie constants of all five materials lie within the range observed experimentally for high-spin transition metal complexes[27] and are in good agreement to those given by Köhler and colleagues.[6,7] Below 50 K, the effective moment of **2**–**4** increase monotonically to a maximum (not shown in the case **2** and **3**). A maximum is observed because of the non-linearity of the magnetization due to spin saturation below the transition temperature.[27]

Ordered state. Curie (or Néel) temperatures (Table 4) were determined by cooling the sample in a field estimated to be less than 0.1 Oe (**2**–**4**) and 7 Oe (**5**). The critical temperature was taken at the point where the magnetization becomes non-zero (Fig. 5). It was also determined by the peak maximum of the dispersive component of the AC measurements in zero DC field. The magnetization data in the vicinity of the transition (T_C–0.8 T_C) for **2**–**4** were fitted to a power law to give a value for the critical exponent β in the range 0.49 ± 0.02.[28] This is close to the value of 0.5 expected for a mean-field ferromagnet. Similar analysis for **5** gave $\beta = 0.37(1)$, considerably different from **2**–**4**. Data lying just above T_C were fitted to give γ'; it

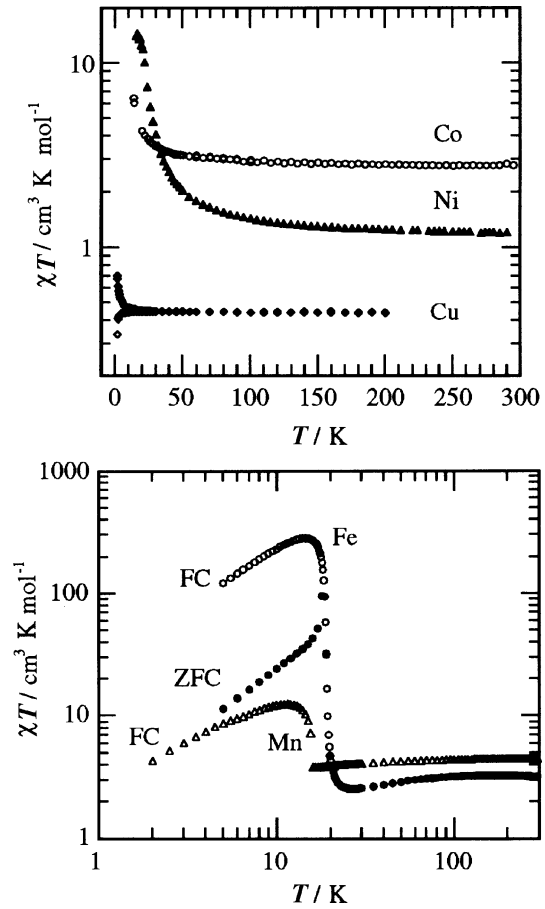

Fig. 4 Temperature dependence of the product χT for (top) $M\{N(CN)_2\}_2$: (◆) M = Cu, alcohol synthesized, $H = 100$ Oe; (◇) M = Cu, water synthesized, $H = 100$ Oe; (▲) M = Ni, $H = 12000$ Oe; (○) M = Co, $H = 12000$ Oe. (bottom) $Fe\{N(CN)_2\}_2$: (●) ZFC and (○) FC, $H = 100$ Oe; (△) $[Mn\{N(CN)_2\}_2(C_2H_5OH)_2]\cdot(CH_3)_2CO$, $H = 7$ Oe

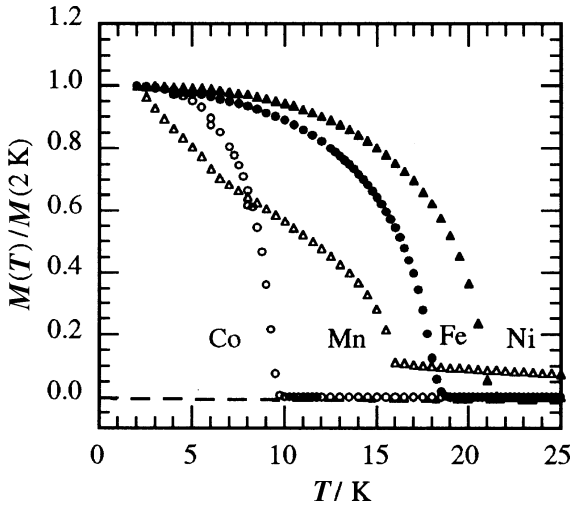

Fig. 5 Temperature dependence of the relative magnetization in an applied field of less than 0.1 Oe for $M\{N(CN)_2\}_2$:(▲) Ni, (○) Co, (●) Fe, and for (△) $[Mn\{N(CN)_2\}_2(C_2H_5OH)_2]\cdot(CH_3)_2CO$ in 7 Oe

was found to be 0.98(3), 0.91(4), 0.29(1) and 0.33(12) for **2**–**5**, respectively. The expected value for a mean field magnet is 1.0. Fits to the high temperature susceptibilities for **2** and **3** gave $\gamma = 1.0 \pm 0.05$. The slight deviation from mean-field behaviour for **2** and **3** is also seen in the value of the Weiss constants (obtained by fitting the data above 50 K), which are marginally larger than the respective transition temperatures (Table 4). The Weiss constant for **2** given by Batten *et al.*[11] is close to ours and is exactly that of the Curie temperature, while that of **3** is surprisingly smaller than its T_C.

AC susceptibilities. The temperature dependence of the AC susceptibilities measured in an applied field of 3 Oe oscillating at 20 Hz are shown in Fig. 6. Each compound is characterized by a symmetric real (dispersive) component (χ') and an asymmetric imaginary (absorptive) component (χ'') of the complex susceptibility. The presence of the imaginary part confirms the existence of magnetic long-range ordering. The decrease of the real part and the highly symmetric peak at T_C indicate that the particles are close to being single domain. The widths of the peaks for **2** and **3** are very similar, whilst those for **4** are approximately halved. The peak intensity for **2** is, as expected, larger than that of **3**, whereas that for **4** is unexpectedly lower. These two anomalies suggest that the magnetic behaviour of **2** and **3** are the same, whilst that of **4** is different. We will take up this point in more detail after discussing the hysteresis loops of the compounds.

No transition was evident from the AC susceptibility measurement of **5**. We attribute this to the sharpness of the transition, and to the low value of the coercive field (which apparently does not exceed 3.5 Oe, the amplitude of the applied AC field). The data between 17 and 300 K can be fitted to a Curie–Weiss law with the same parameters as found from the DC measurements (Table 4).

Table 4 Summary of magnetic data

Compound	**1**[a]	**1**[b]	**2**	**3**	**4**	**5**
M, d^n, Spin (S)	Cu, d^9, 1/2	Cu, d^9, 1/2	Ni, d^8, 1	Co, d^7, 3/2	Fe, d^6, 2	Mn, d^5, 5/2
C/cm³ K mol⁻¹	0.44	0.44	1.21	2.82	3.22	4.54
μ_{eff}/μ_B	1.88	1.88	3.12	4.75	5.07	6.02
Θ/K	0.7(1)	−2.1(4)	22.7(2)	9.7(6)	3(1)	−3.0(1)
T_C/K from:						
M in 0.1 Oe			21.2(2)	9.7(2)	18.5(2)	16.0(2)
χ' in ZF			20.9(1)	9.0(1)	18.8(1)	
C_p in ZF			21.1(4)	9.0(3)	19.0(3)	
β			0.49(2)	0.49(2)	0.49(2)	0.37(1)
γ			1.00(5)	1.00(5)		
γ'			0.98(3)	0.91(4)	0.29(1)	0.33(12)
M/μ_B in [H/T]	1[7]	1[7]	1.98[5]	2.56[5]	1.3[8]	
M_{rem}/μ_B	0	0	1.07	1.45	0.50	0
H_c/Oe at 2 K	0	0	7975	710	17800	<3.5
$(B\cdot H)_{max}/10^6$ G Oe	0	0	26	2	16.6	0
Entropy/J K⁻¹ mol⁻¹			5.6	10.1	4.6	

[a] Synthesized from alcohol; [b]Synthesised from water.

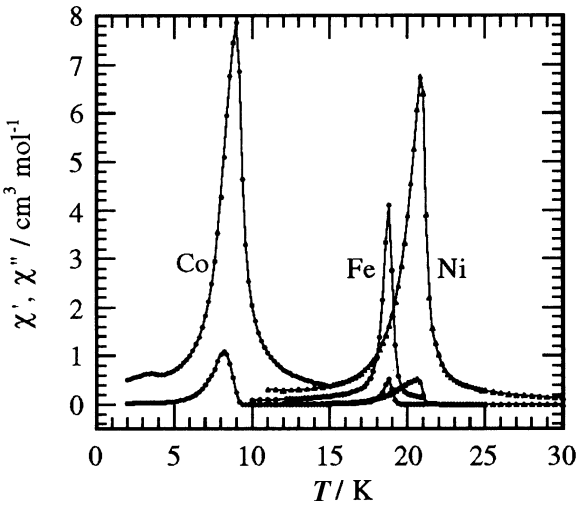

Fig. 6 Temperature dependence of the AC susceptibility for $M\{N(CN)_2\}_2$, M = Ni, Co and Fe, in a field of 3.5 Oe oscillating at 20 Hz

Hysteresis loops. The hysteretic behaviour (magnetization *vs.* field) below the Curie temperatures for compounds **2**, **3** and **4** are shown in Fig. 7. As expected, the field dependence of the magnetization of **1** takes the form of the $J = 1/2$ Brillouin function. Above the Curie temperatures the isothermal magnetization of **2** and **3** are linear down to nearly 2 K above T_C, again confirming mean-field behaviour. Just below T_C, we observe coercive fields and remnant magnetizations. The isothermal magnetization *versus* field has been recorded for **2**–**4** for every degree below the transition temperatures. In each case, we noted an increase of the coercive fields and remnant magnetizations as the temperature is lowered. The results are shown for the case of **3** in Fig. 8(*a*). The remnant magnetization increases in a manner similar to the magnetization in a very small field as shown in Fig. 8(*b*).

The coercive field is strongly dependent on the particle shape and size.[29,30] For example, the cobalt and nickel compounds recrystallized as needles (≈100 μm) from water have coercive fields of <100 and <4000 Oe at 4 K, respectively, whereas those prepared by the ethanol route (fibres of <1 μm) reach fields of 600 and 7000 Oe. The size effect is more dramatic for the iron compound: the coercive field doubles from 8000 to >16 000 Oe at 4 K on simply grinding the compound. The data presented in Fig. 7 and 8(*a*) and those listed in Table 4 were obtained from ground samples prepared by the alcohol

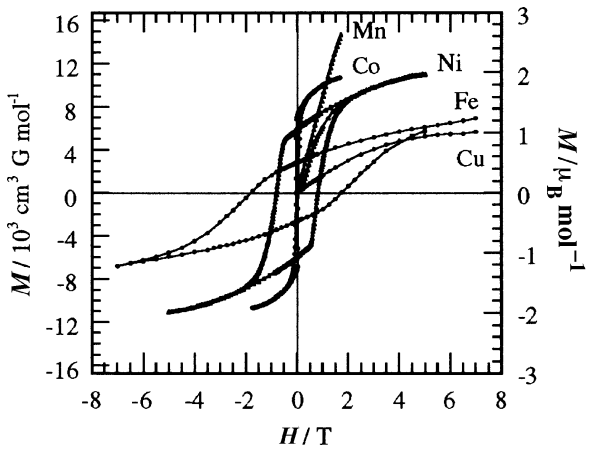

Fig. 7 First magnetization and hysteresis loops (*M vs. H*) for $M\{N(CN)_2\}_2$, M = Cu (T = 2 K), Ni (T = 2 K), Co (T = 4.5 K), Fe (T = 3 K) and for $[Mn\{N(CN)_2\}_2(C_2H_5OH)_2]\cdot(CH_3)_2CO$ (T = 5 K)

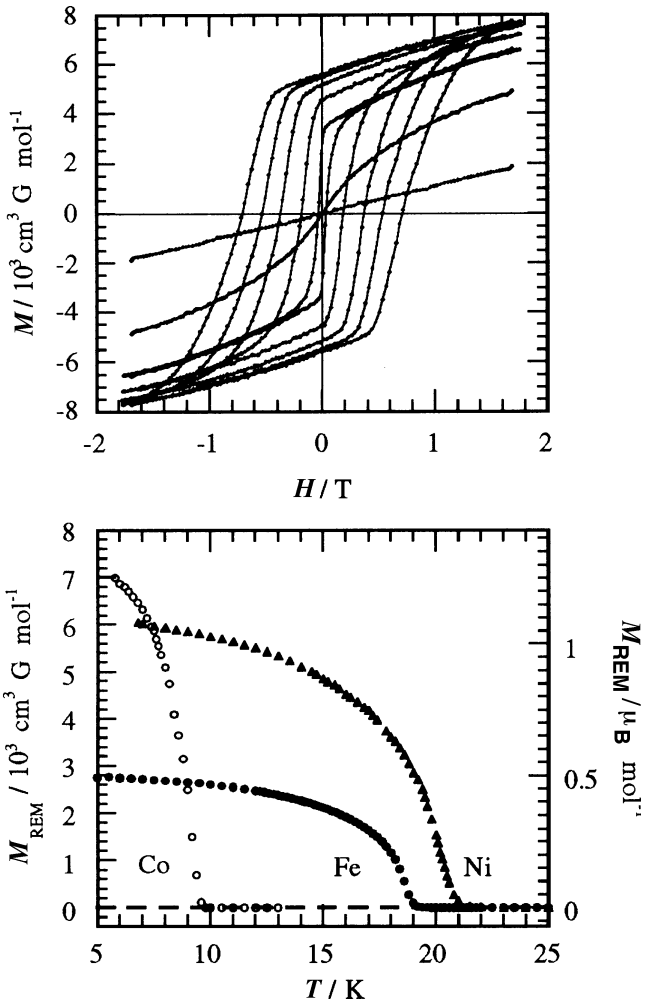

Fig. 8 (top) Temperature dependence of the hysteresis loops for $Ni\{N(CN)_2\}_2$. (bottom) Temperature dependence of the remnant magnetization for $M\{N(CN)_2\}_2$: (▲) Ni, (○) Co, (●) Fe

route. Electron microscopy shows that these samples consisted of very fine cylindrical particles ranging in size from 0.1–0.5 μm. As expected, there is no dependence on synthetic route or crystallite size for the value of the magnetization for fields in the range 5–8 T. The behaviour in this region, namely the slightly lower than expected values of the saturation magnetization and its gradual monotonic increase, characterizes these materials as hard magnets. The saturation magnetization of **2** and **3** tend to the expected values of gS, 2 and 3 μ_B in a field of 5 T, respectively. However, that of **4** is 1.3 μ_B, approximately a third of the expected value (4 μ_B for high spin Fe^{II} assuming spin only and $g = 2$).

This large discrepancy cannot be accounted for by assuming that **4** is a hard magnet and that the applied field is not large enough to achieve saturation. The second anomaly in the behaviour of **4** is that the first magnetization curve has a linear dependence rather than an increasing gradient (as seen in Fig. 7 for the case of **2**). Several hypotheses can be invoked to explain this behaviour. The first is that the effective spin, given the large spin–orbit coupling and the tetragonal distortion, may be reduced to $S = 1/2$; thereby accounting for the value of 1.3 μ_B. The effective spin 1/2 may be achieved since the t_{2g} are the only orbitals affected by spin–orbit coupling described by an orbital quantum number (L) of 1. However, if this is the case the Landé value (g) should be *ca.* 4. The value of the Curie constant (C = 3.22 cm³ K mol⁻¹) does not support this argument. Furthermore, the linear increase of the first magnetization curve is not consistent with the picture of a ferromagnet with a reduced gS. The second hypothesis is

that **4** may be a ferrimagnet having three closely related sublattices (2 having spin up and 1 spin down), if, for example, the magnetic structure adopts the trirutile type. In this case, the saturation magnetization will be 1/3 of 4 μ_B (1.3 μ_B) as observed. However, the shape of the first magnetization curve and the width of the peak in the AC susceptibility are not consistent with this view. One probable explanation for this is that the magnetic structure is that of a canted antiferromagnet. In this case it is difficult to reverse the spin, since the field needed is expected to be larger than that equivalent to the antiferromagnetic exchange field between the sublattices. In our case, a rough estimate of the lower limit from the value of the Weiss constant is >20 T. A canted antiferromagnetic ground state will also explain the linear dependence of the first magnetization, the high coercive field, the sharper and lower value of AC susceptibility peaks and the low value of the critical exponent. Normally, canted antiferromagnets have sharper transitions.[31] From the magnitude of the magnetization, a rough estimate for the canting angle is $\approx 25°$.

Maximum energy product. Given that we have almost square hysteresis loops it is of interest to calculate the maximum energy products ($B \cdot H$) and compare them with those of known hard magnets (Fig. 9).[30] The values we obtained are 2, 26 and 16.6 × 10^6 G Oe for **2**–**4**, respectively. Although these values are at temperatures that are too low for any practical use, they are close to those of alloys of Sm–Co. We consider this is an important breakthrough in this field as it shows promise of achieving better performance magnets from molecular systems. One practical and ecological advantage of these materials is that the cost of materials and manufacturing are very low compared to metallic and alloy systems. Furthermore, the shape anisotropy to reduce the demagnetizing fields is 'generic', being based purely on the molecular structure (the packing of one dimensional rods) and does not need to be optimized through manufacturing processes.

Heat capacity. The temperature dependence of the total specific heats of **2**–**4** are shown in Fig. 10. In each case there is a λ-anomaly reflecting the establishment of long range order at T_C, as determined by the aforementioned techniques. The phonon contribution is expected to be very similar for the three compounds since they are isostructural. The lattice contribution has been estimated from the plot of C_p/T *vs.* T^2, and the magnetic contribution obtained by subtracting the lattice part from the total. The entropy was therefore calculated by integration of the C_p/T *vs.* T plot. The values, 5.6, 10.1 and 4.6 J K^{-1} mol^{-1} for **2**–**4**, respectively, are lower than expected $\{R \ln(2S + 1)\}$. We are unable to perform measurements on **5**

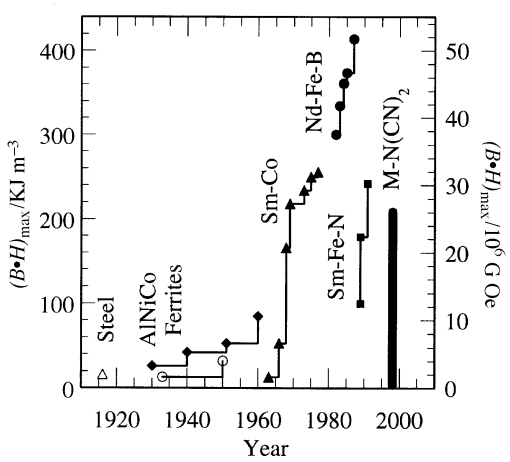

Fig. 9 Historic development of magnets represented by the time evolution of the maximum energy product

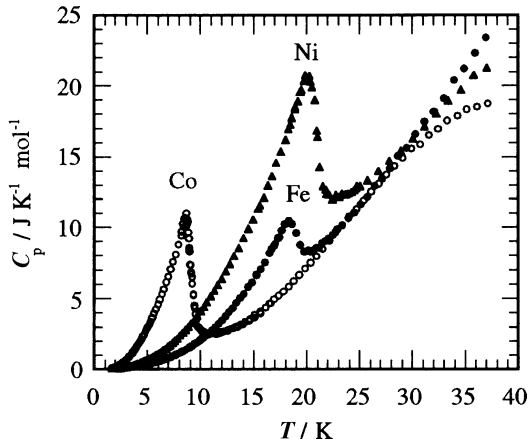

Fig. 10 Temperature dependence of the specific heat of M{N(CN)$_2$}$_2$: (▲) Ni, (○) Co, (●) Fe.

due to loss of solvent of crystallization in the high vacuum needed in the sample port. The shape of the observed λ peaks for **2** and **3** after removal of the lattice contribution are consistent with that expected for mean-field magnets.

Discussion

The unit cell volumes for the isostructural salts $M^{II}\{N(CN)_2\}_2$ are closely similar, the small differences being attributable to variation of the ionic radii of Co^{II}, Ni^{II} and Cu^{II}. This observation, accompanied by calculations of void volumes with PLATON,[16] suggests that the atoms are efficiently packed in a rutile-type structure. The large Jahn–Teller distortion about Cu^{II} in **1** has a strong influence on the geometry of the framework structure, leading to a considerable decrease in the angle between neighbouring ribbons (52.3° compared to 58.8° in **3**). The lattice is slightly compressible, and the T_C of **3** is increased from 21 to 22.6 K on application of an isotropic pressure of 17 kbar.[32] In these salts, the dicyanamide ligand is triply coordinating through its three nitrogen atoms, the first time such an arrangement has been observed. Previously, dicyanamide had been seen to adopt three different types of bonding: coordinating *via* one terminal nitrogen, bridging two metal atoms *via* the two terminal nitrogen atoms, and bridging four metal atoms such that one of the terminal nitrogen atoms is doubly coordinating. It shows considerable π–π interactions in the compounds Ni(en)$_2${N(CN)$_2$}$_2$ and in Cu(Meim)$_4${N(CN)$_2$}$_2$.[19]

Despite forming an isostructural series, there is considerable variation in the magnetic properties of **1**–**4**. An interesting question is what differences may account for **1** being paramagnetic, **2** and **3** being ferromagnetic, and **4** being a canted antiferromagnet. For compounds having the rutile structure, Goodenough[33] has proposed a phase diagram that consists of four possible ground states depending on the ratio of the exchange interactions. In the present rutile-type structure there are four independent nearest-neighbour magnetic-exchange interactions: eight equivalent super-exchange (J_d, d for diagonal) *via* M1—N1—C1—N2···M1′ (M···M′ of 5.94 Å), two equivalent direct (J_a) along *a* at 5.98 Å and two (J_b) along *b* at 7.11 Å and a further two that are a combination of direct and super-exchange (J_c) along *c* at 7.34 Å. Within this structure type the magnetic ground state and Curie temperature, and therefore the magnitudes and signs of the magnetic exchange interactions, are found to depend greatly on the M—N coordination distances and on the degree of structural distortion. The absence of any clear relationship between the Curie temperature and the metal spin state for the different transition metals provides further evidence for the fine dependence of the magnetic behaviour on the structure rather

than the metal spin state alone. The relatively weak magnetic exchange in **1** is likely to reflect a severe weakening of the J_d interaction due to the Jahn–Teller distortion about the Cu^{II} ion, and indicates that the other exchange interactions are weak. Furthermore, this observation suggests that it is the approximate orthogonal super-exchange pathway, J_d, that is highest in magnitude for **2**–**4**. We propose that it is a strong and positive J_d in both **2** and **3** that is responsible for the moderate temperature ferromagnetism in these materials.

Compounds **2** and **3** have almost identical structures, and both behave as mean-field magnets. Comparing the data of these salts, there are two anomalies to be noted. The Curie temperature is expected to vary as $S(S + 1)$, but does in fact follow the reverse behaviour. This may reflect the argument that the magnitude of, and therefore the competition between different exchange interactions, depends strongly on the structure. Secondly, octahedral Co^{II} has a larger orbital contribution and therefore a higher anisotropy than Ni^{II}, and so **3** might be expected to have a larger coercive field than **2**. One possible reason for the opposite behaviour observed may be the synergy of the parallel alignment of magnetocrystalline anisotropy and shape anisotropy in **2** but perpendicular alignment in **3**.

There are several possible reasons for the observation of canted antiferromagnetism in the Fe complex (**4**). In the relatively weak, pseudo-octahedral ligand field, the $3d^6$ electronic configuration is expected to give rise to the $^5T_{2g}$ ground state. With two electrons in the t_{2g} orbitals and two in the e_g there will be an equivalent number of antiferromagnetic and ferromagnetic interactions, the former presumably being the larger in magnitude since an antiferromagnetic ground state is established at low temperature. Since spin–orbit coupling is large for Fe^{II}, antisymmetric exchange is likely to cause a canting of the sublattices according to the Dzyaloshinskii–Moriya mechanism.[34] With only one metal site in the crystallographic asymmetric unit, however, such a mechanism cannot operate. This points to the possibility that the structure of **4** is based on trirutile, like that of WCr_2O_6,[22,35] which can accommodate three slightly different metal sites. The resolution of a trirutile structure from that of a normal rutile is difficult from powder diffraction data due to the near equivalence of the three layers within the tripled cell. Given the poor quality of the X-ray powder diffraction pattern, which resembles that of the fine powder of the cobalt and nickel complexes, we cannot comment further on this possible structural modulation.

Due to the similarities in behaviour of **5** to the 2D-polymeric canted antiferromagnets, $Co\{pyrimidine\}_2(NCS)_2$ and $Mn\{SCN\}_2(C_2H_5OH)_2$, we propose a similar layer structure for $[Mn\{N(CN)_2\}_2(C_2H_5OH)_2]\cdot(CH_3)_2CO$.[12] The lower value of χT [Fig. 4(*b*)] at the maximum for **5** than for **4** implies that the canting angle is smaller, in good agreement with the fact that the spin–orbit coupling for Mn^{II} is smaller than for Fe^{II}. Consequently, the mechanism for canting is by second-order effects. Further crystallographic and electron paramagnetic resonance studies are in progress to elucidate the mechanism and magnitude of the canting.

The cyanide and polycyanide ligands first emerged as good building units for constructing magnetic materials when it was[36] demonstrated that high critical temperature magnets can be achieved by the appropriate choice of metals in the Prussian blue family and Manriquez *et al.*[37] observed that $V(TCNE)_2\cdot$solvent is a room temperature magnet. Salts of the families $M^{II}(TCNQ)_x$[38] and $M^{II}(TCNE)_x$[39] have more recently been reported to show magnetically ordered ground states over a wide range of temperatures (including one above room temperature), although poor crystallinity has hampered their crystallographic characterisation. In contrast, the highly crystalline polycyanide salts $M^{II}\{C(CN)_3\}_2$ (M = Cu, Ni, Co, Fe and Mn) are dominated by antiferromagnetic interactions.[23] Amongst the different families of transition metal-polycyanide complexes, the dicyanamides represent an ideal system for study, providing a rich diversity of magnetic properties, which range from paramagnetic to canted antiferromagnetic to ferromagnetic, and being among the most crystalline for the purpose of structural characterization.

Conclusions

The dicyanamide anion is well-suited to aligning divalent transition metals in such a way that their magnetic orbitals are approximately orthogonal. The reaction proceeds though a self-assembly of the M^{II} and the $N(CN)_2^-$ to give tetragonally distorted octahedra, the $N(CN)_2^-$ adopting an unprecedented triple coordination. The magnetic ground states of metal salts of this anion depend on the electronic configurations and on the geometry-dependent balance between ferromagnetic and antiferromagnetic interactions. Compounds **2** and **4** have the largest coercive field (7975 and 17 800 Oe, respectively) of all known metal-organic magnets, as a result of the synergy of parallel alignment of the magnetocrystalline anisotropy and the shape anisotropy. This study demonstrates that, in the design and synthesis of new metal-organic magnets, the organic ligand should be multidentate to bind to several metals, be small to promote direct exchange interactions between the moments, and have delocalized electronic densities (*e.g.*, π electrons) to enhance indirect exchange between metal sites. The shape and positions of the binding sites in the ligand are crucial in the organization of the metals around it.

Acknowledgements

We thank A. Derory, R. Poinsot, M. Richard-Plouet and J. P. Lambour for technical assistance, Professor C. K. Prout and Dr. D. J. Watkin for access to the single crystal X-ray diffractometer, Professor K. Prassides for solving the structure of the cobalt complex from the neutron diffraction and Dr. A. Traverse for the help with EXAFS. We are grateful for useful discussions with Drs. P. Panissod, M. Drillon, C. Mathoniére and Professors P. Day, O. Kahn and T. Mallah. We thank Professors. J. S. Miller and A. J. Epstein for communicating their results prior to publication. This work was supported by the CNRS (France). CJK thanks Christ Church, Oxford, for a Junior Research Fellowship.

References

1 (*a*) *Magnetism: A Supramolecular Function*, ed. O. Kahn, NATO ASI Series C484, Kluwer, Dordrecht, 1996, pp. 1–645; (*b*) B. F. Hoskins and R. Robson, *J. Am. Chem. Soc.*, 1990, **112**, 1546; (*c*) B. F. Abrahams, S. R. Batten, H. Hamit, B. F. Hoskins and R. Robson, *Chem. Commun.*, 1996, 1313; (*d*) B. F. Abrahams, S. J. Egans, B. F. Hoskins and R. Robson, *Chem Commun.*, 1996, 1099; (*e*) B. F. Abrahams, B. F. Hoskins, D. M. Michael and R. Robson, *Nature* (*London*), 1994, **369**, 727; (*f*) C. J. Kepert and M. J. Rosseinsky, *Chem. Commun.*, 1998, 31; (*g*) O. M. Yaghi, G. M. Li and H. L. Li, *Nature* (*London*), 1995, **378**, 703; (*h*) O. M. Yaghi, C. E. Davis, G. M. Li and H. L. Li, *J. Am. Chem. Soc.*, 1997, **119**, 2861; (*i*) K. A. Hirsch, S. R. Wilson and J. S. Moore, *Chem. Commun.*, 1998, 13; *Chem. Eur. J.*, 1997, **3**, 765; (*j*) G. A. Ozin and C. L. Bowes, *Adv. Mater.*, 1996, **8**, 13; (*k*) W. Fujita, Y. L. Kwon, S. Washizu and K. Ogura, *J. Am. Chem. Soc.*, 1994, **116**, 1151; (*l*) H. O. Stumpf, L. Ouahab, Y. Pei, D. Grandjean and O. Kahn, *Science*, 1993, **261**, 447; (*m*) G. A. Ozin, *Adv. Mater.*, 1992, **4**, 612; (*n*) J.-F. Nicoud, *Science*, 1994, **263**, 638; (*o*) M. C. Etter, *Acc. Chem. Res.*, 1990, **23**, 120.

2 (*a*) M. Kurmoo, P. Day, P. Guionneau, G. Bravic, D. Chasseau, L. Ducasse, M. L. Allan, I. D. Marsden and R. H. Friend, *Inorg. Chem.*, 1996, **35**, 4719; (*b*) C. J. Kepert, M. Kurmoo and P. Day, *Inorg. Chem.*, 1997, **36**, 1128; (*c*) C. J. Kepert, M. Kurmoo and P. Day, *J. Mater. Chem.*, 1997, **7**, 221; (*d*) P. Day, M. Kurmoo, T. Mallah, I. R. Marsden, R. H. Friend, F. L. Pratt, W. Hayes, D. Chasseau, J. Gaultier, G. Bravic and L. Ducasse, *J. Am. Chem.*

Soc., 1992, **114**, 10722; (*e*) I. D. Marsden, M. L. Allan, R. H. Friend, M. Kurmoo, D. Kanazawa, P. Day, D. Chasseau, G. Bravic and L. Ducasse, *Phys. Rev. B*, 1994, **50**, 2118.
3 M. Kurmoo, A. W. Graham, P. Day. S. Coles, M. B. Hursthouse, J. L. Caulfield, J. Singleton, F. L. Pratt, W. Hayes, L. Ducasse and P. Guionneau, *J. Am. Chem. Soc*., 1995, **117**, 12209.
4 (*a*) A. M. Kini, U. Geiser, H. H. Wang, K. D. Carlson, J. M. Williams, W. K. Kwok, K. G. van Dervoort, J. E. Thompson, D. L. Stupka, D. Jung and M.-H. Whangbo, *Inorg. Chem*., 1990, **29**, 2555; (*b*) U. Geiser, A. M. Kini, H. H. Wang, M. A. Beno and J. M. Williams, *Acta Crystallogr*., *Sect. C*, 1991, **47**, 190.
5 T. Komatsu, H. Sato, T. Nakamura, N. Matsukawa, H. Yamochi, G. Saito, M. Kusonoki, K. Sakaguchi and S. Kagoshima, *Bull. Chem. Soc. Jpn*., 1995, **68**, 2233.
6 H. Köhler, H. Hartnung and A. M. Golub, *Z. Anorg. Allg. Chem*., 1974, **403**, 41.
7 (*a*) H. Köhler, *Z. Anorg. Allg. Chem*., 1964, **331**, 237; (*b*) H. Köhler and B. Seifert, *Z. Anorg. Allg. Chem*., 1966, **344**, 63; (*c*) A. J. Civadze and H. Köhler, *Z. Anorg. Allg. Chem*., 1984, **510**, 31; (*d*) H. Köhler, A. Kolbe and G. Z. Lux, *Z. Anorg. Allg. Chem*., 1977, **428**, 103.
8 (*a*) J. N. McElearney, L. L. Balagot, J. A. Muir and R. D. Spence, *Phys. Rev. B*, 1979, **19**, 306; (*b*) G. C. DeFotis, E. D. Remy and C. W. Scherrer, *Phys. Rev. B*, 1990, **41**, 9074; (*c*) G. C. DeFotis, E. W. Harlan, E. D. Remy and K. D. Dell, *J. Appl. Phys*., 1991, **69**, 6004.
9 F. Lloret, G. De Munno, M. Julve, J. Cano, R. Ruiz and A. Caneschi, *Angew. Chem., Int. Ed. Engl*., 1998, **37**, 135.
10 (*a*) J. Kohout, M. Hvastijova, H. Köhler and L. Omelka, *Collect. Czech. Chem. Commun*., 1990, **55**, 435; (*b*) M. Hvastijova, *Collect. Czech. Chem. Commun*., 1994, **59**, 2611; (*c*) M. Hvastijova, J. Kohout, J. Mrozinski and L. Jager, *Pol. J. Chem*., 1995, **69**, 852; (*d*) M. Hvastijova, J. Kohout and H. Köhler, *Monatsh. Chem*., 1992, **123**, 493; (*e*) M. Hvastijova, J. Kohout, H. Wusterhausen and H. Köhler, *Z. Anorg. Allg. Chem*., 1984, **510**, 37; (*f*) J. Mrozinski, M. Hvastijova and J. Kohout, *Polyhedron*, 1992, **11**, 2867.
11 S. R. Batten, P. Jensen, B. Moubaraki, K. S. Murray and R. Robson, *Chem. Commun*., 1998, 439.
12 Z. Otwinowski and W. Minor, in *Methods in Enzymology*, eds. C. W. Carter, R. M. Sweet, Academic Press, London, 1996, p. 276.
13 G. M. Sheldrick, *SHELXS-86*, *Program for Crystal Structure Determination*, Universität Göttingen, 1986.
14 G. M. Sheldrick, *SHELXL-93*, *Program for Crystal Structure Refinement*, Universität Göttingen, 1993.
15 (*a*) P. E. Werner, *Z. Kristallogr*., 1964, **120**, 375; (*b*) A. Boutif and D. Loüer, *J. Appl. Crystallogr*., 1991, **24**, 987.
16 A. L. Spek, *Acta Crystallogr*., *Sect. A*, 1990, **46**, 194.
17 F. H. Allen and O. Kennard, *Chem. Des. Auto. News*, 1993, **8**, 1; *ibid*., 31.
18 (*a*) P. Starynowicz, *Acta Crystallogr*., *Sect. C*, 1991, **47**, 2198; (*b*) X. Bu, P. Coppens, B. Lederle and M. J. Naughton, *Acta Crystallogr*., *Sect. C*, 1992, **48**, 1590.
19 (*a*) K. Lattaud and M. Kurmoo, unpublished results; (*b*) I. Potocnak, M. Dunaj-Jurco, D. Miklos, M. Kabesova and L. Jager, *Acta Crystallogr*., *Sect. C*, 1995, **51**, 600; (*c*) I. Potocnak, M. Dunaj-Jurco, D. Miklos and L. Jager, *Acta Crystallogr*., *Sect. C*, 1996, **52**, 1653.
20 (a) V. V. Skopenko, A. O. Kapshuk and F. G. Kramarenko, *Dokl. Akad. Nauk. Ukr. RSR, Ser. B Fiz. Mat. Tek. Nauki*, 1982, 73; (b) A. A. Kapshuk and V. V. Skopenko, *Koord. Khim*., 1986, **12**, 380; (c) D. Britton, *Acta Crystallogr*., *Sect. C*, 1990, **46**, 2297; (d) D. Britton and Y. M. Chow, *Acta Crystallogr*., *Sect. B*, 1977, **33**, 697; (e) Y. M. Chow, *Inorg. Chem*., 1971, **9**, 1938.
21 Y. M. Chow and D. Britton, *Acta Crystallogr*., *Sect. B*, 1975, **31**, 1934.
22 A. F. Wells, *Structural Inorganic Chemistry*, Clarendon Press, Oxford, 1975.
23 (*a*) S. R. Batten, B. F. Hoskins and R. Robson, *J. Chem. Soc*., *Chem. Commun*., 1991, 445; (*b*) J. L. Manson, C. Campana and J. S. Miller, *Chem. Commun*., 1998, 251.
24 A. Michalowicz, Ph.D. Thesis, Université Paris XII, Créteil, 1990.
25 *Chemistry of Pseudohalides*, eds. A. M. Golub, H. Köhler and V. V. Skopenko, Elsevier, Amsterdam, 1986.
26 (*a*) B. N. Figgis, *Introduction to Ligand Fields*, John Wiley, London, 1966; (*b*) F. E. Mabbs and D. J. Machin, *Magnetism and Transition Metal Complexes*, Chapman and Hall, London, 1973.
27 (*a*) A. Herpin, *Theorie du Magnetisme*, Presse Universitaire de France, Paris, 1968; (*b*) O. Kahn, *Molecular Magnetism*, VCH, New York, 1993.
28 (*a*) C. Domb, *The Critical Point*, Taylor Francis, London, 1996; (*b*) H. E. Stanley, *Introduction to Phase Transitions and Critical Phenomena*, Clarendon Press, Oxford, 1971.
29 S. Chikazumi, *Physics of Magnetism*, John Wiley, New York, 1964.
30 (*a*) J. M. D. Coey, *Solid State Commun*., 1997, **102**, 101; (*b*) *Supermagnets*, *Hard Magnetic Materials*, eds., G. J. Long and F. Grandjean, NATO ASI Series C331, Kluwer, Dordrecht, 1991, pp. 1–69, and references therein.
31 (*a*) H. A. Groenendijk, , Ph.D. thesis, University of Leiden, 1981; (*b*) H. A. Groenendijk, A. J. van Duyneveldt and R. L. Carlin, *Physica B&C*, 1982, **115**, 63; (*c*) H. A. Groenendijk and A. J. van Duyneveldt, *Physica B&C*, 1982, **115**, 41.
32 Y. Iwasa and M. Kurmoo, unpublished results.
33 J. B. Goodenough, *Magnetism and the Chemical Bond*, John Wiley and Sons, New York, 1963.
34 (*a*) I. Dzyaloshinskii, *J. Phys. Chem. Solids*, 1958, **4**, 241; (*b*) T. Moriya, *Phys. Rev*., 1960, **120**, 91.
35 G. Bayer, *J. Am. Ceram. Soc*., 1960, **43**, 495.
36 (*a*) V. Gadet, T. Mallah, I. Castro and M. Verdaguer, *J. Am. Chem. Soc*., 1992, **114**, 9213; (*b*) T. Mallah, S. Thiebaut, M. Verdaguer and P. Veillet, *Science*, 1993, **262**, 1554; (*c*) W. R. Entley and G. S. Girolami, *Science*, 1995, **268**, 397; (*d*) D. Babel, *Inorg. Chem*., 1986, **5**, 285; (*e*) N. Vernier, G. Bellessa, T. Mallah and M. Verdaguer, *Phys. Rev. B*, 1997, **56**, 75.
37 J. M. Manriquez, G. T. Yee, R. S. McClean, A. J. Epstein and J. S. Miller, *Science*, 1991, **252**, 1415.
38 (*a*) V. J. Murphy and D. O'Hare, *Inorg. Chem*., 1994, **33**, 1833; (*b*) C. Campana, K. R. Dunbar and X. Ouyang, *Chem. Commun*., 1996, 2427; (*c*) H. Zhao, R. A. Heintz and K. R. Dunbar, *J. Am. Chem. Soc*., 1996, **118**, 12844; (*d*) H. Oshio, E. Ino, T. Ito and Y. Maeda, *Bull. Chem. Soc. Jpn*., 1995, **68**, 889.
39 (*a*) K. R. Dunbar, *Angew. Chem., Int. Ed. Engl*., 1996, **35**, 1659; (*b*) K. R. Dunbar and R. A. Heintz, *Prog. Inorg. Chem*., 1997, **45**, 283; (*d*) K. R. Dunbar and X. Ouyang., *Mol. Cryst. Liq. Cryst*., 1995, **273**, 21; (*e*) J. Zhang, J. Ensling, V. Ksenofontov, P. Gütlich, A. J. Epstein and J. S. Miller, *Angew. Chem., Int. Ed. Engl*., 1998, **37**, 6570.

Received in Strasbourg, France, 24th April 1998;
Paper 8/03165G